Supporting Information

Nonfullerene Acceptor for Organic Solar Cells with Chlorination on Dithieno[3,2-*b*:2′,3′-*d*]pyrrol Fused-Ring

Renyong Geng,[†,⊥] Xin Song,[‡,⊥] Haohao Feng,[†] Jiangsheng Yu,[§] Ming Zhang,[¶] Nicola Gasparini,[‡] Zhuohan Zhang,[†] Feng Liu,[*,¶] Derya Baran,[*,‡] and Weihua Tang[*,†]

[†]School of Chemical Engineering, Nanjing University of Science and Technology, Nanjing 210094, China
[‡]KAUST Solar Center (KSC), King Abdullah University of Science and Technology (KAUST), Thuwal 23955-6900, Saudi Arabia
[¶]MIIT Key Laboratory of Advanced Solid Laser, Nanjing University of Science and Technology, Nanjing 210094, China
[§]Department of Physics and Astronomy, Collaborative Innovation Center of IFSA, Shanghai Jiao Tong University, Shanghai 200240, China

Table of Content

1. Materials and Synthesis

Unless stated otherwise, all commercially available chemicals and solvents were used directly without further purification. Tetrahydrofuran (THF) and toluene were distilled from sodium before use, and 1,2-dichloroethane was dried with calcium hydride. 2-(5,6-Dichloro-3-oxo-2,3-dihydro-1H-inden-1-ylidene) malononitrile (2Cl-IC) was synthesized according to the literature,[S1] while 2-(3-oxo-2,3-dihydro-1*H*-inden-1-ylidene) malononitrile (IC) and 2-(5,6-difluoro-3-oxo-2,3-dihydro-1H-inden-1-ylidene) malononitrile (2F-IC) were purchased from Derthon Optoelectronic Materials Science Technology Co. LTD.

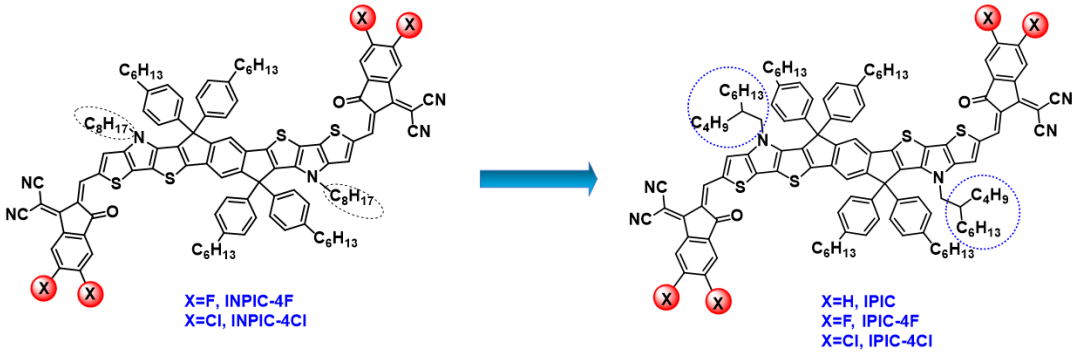

Scheme S1. Molecule design approach for the halogenated IPIC based nonfullerene acceptors.

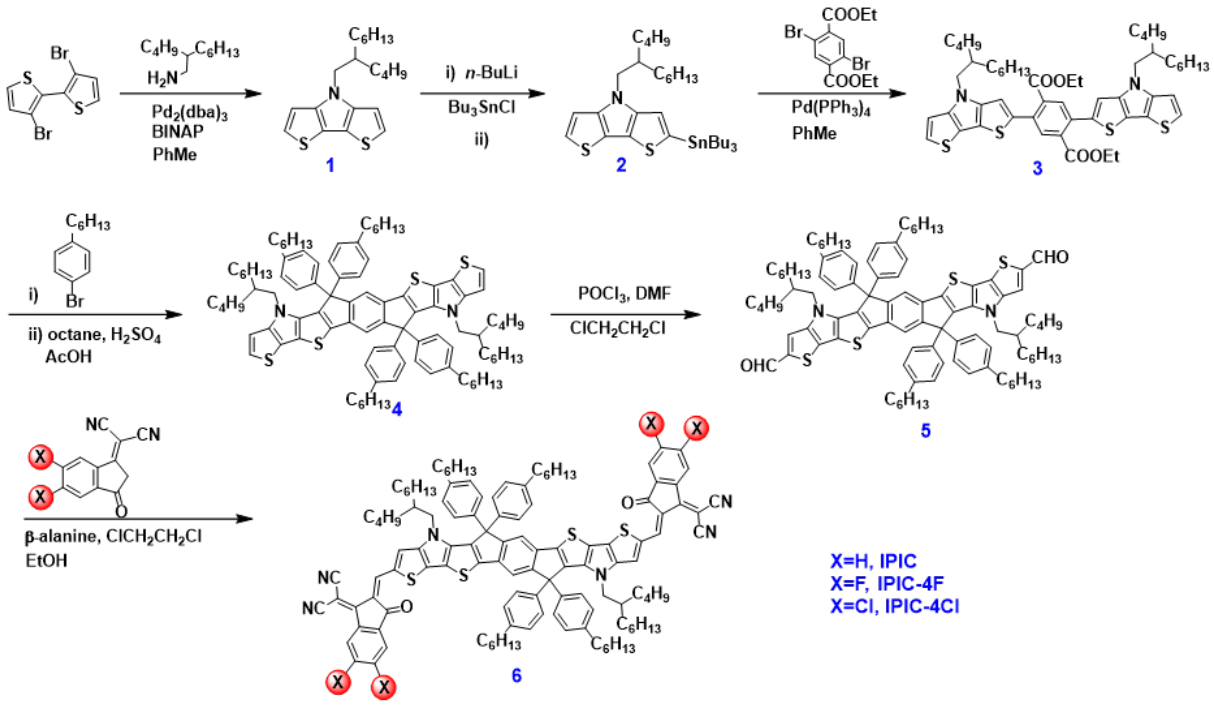

Scheme S2. Synthetic route to different halogenated IPIC-based acceptors.

*Synthesis of compound **1***

A solution of 3,3'-dibromo-2,2'-bithiophene (3.00 g, 9.26 mmol), sodium tert-butoxide (2.67

g, 27.77 mmol), tris(dibenzylideneacetone) dipalladium [$Pd_2(dba)_3$, 0.25 g, 0.28 mmol], and BINAP (0.58 g, 0.93 mmol) in dry toluene (20 mL) was purged with nitrogen. After 20 min, *2-butyloctan-1-amine* (1.73 g, 9.35 mmol) was added. After refluxing at 110 °C overnight, the organic layer was extracted with ethyl acetate (3×100 mL) and washed with water for three times. The combined organic phase was dried over anhydrous $MgSO_4$. After solvent removal, the residue was purified using column chromatography on silica gel using petroleum ether/dichloromethane (10:1, v/v) as the eluent. The *title* compound was obtained as a yellow solid (2.60 g, 80 %). ^{1}H NMR (500 MHz, $CDCl_3$, δ): 7.12 (d, *J* = 5.3 Hz, 2H), 6.97 (d, *J* = 5.3 Hz, 2H), 4.05 (d, *J* = 7.3 Hz, 2H), 1.34-1.20 (m, 17H), 0.89-0.84 (m, 6H).

*Synthesis of compound **2** and **3***

Compound **1** (1.50 g, 4.32 mmol) was dissolved in freshly distilled THF (20 mL) at -78 °C. *n*-BuLi (1.73 mL, 4.32 mmol, 2.5 M in hexane) was added into the above solution dropwise over 10 min under nitrogen. After stirring at -78 °C for 1.5 h, tributyltin chloride (1.55 g, 4.75 mmol) was added dropwise over 5 min. The solution was then warmed to room temperature. After stirring for another 3 h, water was added to quench the reaction. The reaction mixture was extracted with diethyl ether twice, with the organic layers dried over anhydrous $MgSO_4$. After solvent removal, compound **2** was obtained and used directly without further purification.

Compound **2**, diethyl 2,5-dibromoterephthalate (0.71 g, 1.88 mmol), $Pd(PPh_3)_4$ (43.41 mg, 37.56 μmol) were added in anhydrous toluene (20 mL). The mixture was then refluxed for 18 h under nitrogen. After general work-up, the crude product was purified by silica gel column chromatography (petroleum ether/dichloromethane =3:2 v/v) to afford a brown solid (1.23g, 72%). ^{1}H NMR (500 MHz, $CDCl_3$, δ): 7.84 (s, 2H), 7.16 (d, *J* = 5.3 Hz, 2H), 7.04 (s, 2H), 6.98 (d, *J* = 5.3 Hz, 2H), 4.25 (d, *J* = 7.1 Hz, 4H), 4.05 (d, *J* = 7.4 Hz, 4H), 1.36-1.19 (m, 34H), 1.14 (m, 6H), 0.91-0.81 (m, 12H). ^{13}C NMR (125 MHz, $CDCl_3$, δ): 168.45, 145.37, 145.27, 137.55, 134.10, 133.92, 131.69, 123.75, 115.99, 114.92, 111.23, 61.90, 52.04, 39.30, 31.98, 31.83, 31.51, 29.79, 28.90, 26.68, 23.19, 22.81, 14.23, 14.17. MALDI-TOF MS (*m*/*z*): $[M + H]^+$ calcd. for $C_{52}H_{68}N_2O_4S_4$, 912.4062; found, 912.4059.

*Synthesis of compound **4***

n-BuLi (2.63 mL, 6.57 mmol, 2.5 M in hexane) was added in a solution of 4-hexyl-1-bromobenzene (1.58 g, 6.57 mmol) in anhydrous THF (10 mL) at -78 °C. After the reaction mixture was stirring for 1 h at -78 °C, compound **3** (1.0 g, 1.09 mmol) in THF (30 mL) was then added slowly. After stirring at room temperature overnight, the reaction mixture was poured into water and extracted twice with ethyl acetate. The combined organic phase was dried

over anhydrous Na_2SO_4. The solvent was evaporated, and yellow residue was dissolved in octane (100 mL) and acetic acid (10 mL), then concentrated H_2SO_4 (0.5 mL) was added dropwise slowly. The solution was stirred at 65 °C for 4 h before quenched by water. The organic layer was extracted with ethyl acetate (3×100 mL) and washed with water for three times. The combined organic phase was dried over anhydrous $MgSO_4$. After solvent removal, the residue was purified using column chromatography on silica gel employing petroleum ether/dichloromethane (10:1, v/v) as the eluent. The *title* compound was obtained as a yellow solid (0.96 g, 61%). ^{1}H NMR (500 MHz, $CDCl_3$, δ): 7.30 (dd, *J* = 8.3, 2.7 Hz, 8H), 7.27 (s, 2H), 7.07-7.02 (m, 10H), 6.88 (d, *J* = 5.2 Hz, 2H), 3.58 (d, *J* = 8.2 Hz, 4H), 2.58-2.51 (m, 8H), 1.59-1.54 (m, 8H), 1.35-1.24 (m, 28H), 1.18 (m, 5H), 1.11-0.96 (m, 13H), 0.95-0.89 (m, 4H), 0.89-0.78 (m, 24H), 0.73 (t, 6H), 0.64-0.53 (m, 8H). ^{13}C NMR (125 MHz, $CDCl_3$, δ): 156.59, 144.40, 141.86, 141.21, 141.05, 139.86, 139.04, 135.69, 129.32, 128.51, 122.30, 117.58, 116.58, 114.71, 112.57, 62.85, 53.00, 37.63, 35.78, 31.95, 31.60, 30.95, 30.69, 29.71, 29.39, 29.22, 26.93, 23.08, 22.81, 14.31, 14.19. MALDI-TOF MS (*m*/*z*): $[M+H]^+$ calcd. for $C_{96}H_{124}N_2S_4$, 1432.8647; found, 1432.8656.

*Synthesis of compound **5***

Phosphorus oxychloride ($POCl_3$, 0.3 mL) was dropped in a solution of compound **4** (600 mg, 0.42 mmol) in dry 1,2-dichloroethane ($ClCH_2CH_2Cl$, 20 mL) and DMF (5 mL) at 0 °C under nitrogen. The mixture was stirred at 0 °C for 1 h. After refluxing at 85 °C overnight, the mixture was poured into ice water (100 mL) and neutralized with Na_2CO_3 (aq). The reaction mixture was extracted with dichloromethane. The combined organic layer was washed with water and brine, dried over anhydrous Na_2SO_4. After solvent removal, the crude product was purified by silica gel using petroleum ether/dichloromethane (3:2, v/v) as eluent. The *title* compound was obtained as an orange solid (480 mg, 77%). ^{1}H NMR (500 MHz, $CDCl_3$, δ): 9.82 (s, 2H), 7.49 (s, 2H), 7.35 (s, 2H), 7.28 (d, *J* = 6.0 Hz, 8H), 7.08 (d, *J* = 7.9 Hz, 9H), 3.63 (d, *J* = 8.2 Hz, 4H), 2.58-2.54 (m, 8H), 1.58 (d, *J* = 7.6 Hz, 10H), 1.37-0.90 (m, 59H), 0.89-0.80 (m, 26H), 0.74 (t, 6H), 0.64-0.55 (m, 8H). ^{13}C NMR (125 MHz, $CDCl_3$, δ): 182.82, 157.37, 146.42, 145.32, 143.88, 142.40, 139.73, 139.52, 138.18, 136.03, 129.12, 128.73, 125.13, 120.72, 118.14, 115.54, 62.97, 53.11, 37.91, 35.74, 31.91, 31.56, 30.95, 30.72, 29.71, 29.36, 29.20, 26.92, 23.08, 22.78, 14.28, 14.15. MALDI-TOF MS (*m*/*z*): $[M+H]^+$ calcd. for $C_{98}H_{124}N_2O_2S_4$, 1488.8546; found, 1488.8547.

*Synthesis of **IPIC- 4Cl***

Compound **5** (150.0 mg, 100.65 μmol), 2Cl-IC (211.83 mg, 0.81 mmol) and β-alanine (1.94

mg, 21.77 μmol) were dissolved in a mixture of $ClCH_2CH_2Cl$ and EtOH (6 mL/3 mL). The rigorously stirred mixture was refluxed overnight. After extracted with chloroform, the resulting mixture was washed with water and dried over anhydrous $MgSO_4$. After removal of solvent, the crude product was purified on a silica-gel column chromatography with petroleum ether/dichloromethane (2:1, v/v) as eluent. The *title* compound IPIC-4Cl was obtained as a black-green solid (156 mg, 78%). ^{1}H NMR (500 MHz, $CDCl_3$, δ): 8.81 (s, 2H), 8.68 (s, 2H), 7.87 (s, 2H), 7.58 (s, 2H), 7.42 (s, 2H), 7.28 (m, 8H), 7.12 (d, *J* = 8.2 Hz, 8H), 3.63 (d, *J* = 8.2 Hz, 4H), 2.62-2.55 (m, 8H), 1.62-1.56 (m, 8H), 1.38-0.91 (m, 42H), 0.91-0.69 (m, 24H), 0.66-0.57 (m, 8H). ^{13}C NMR (125 MHz, $CDCl_3$, δ): 186.02, 158.49, 152.51, 149.40, 146.87, 142.90, 139.60, 138.96, 138.69, 138.56, 137.43, 136.75, 136.47, 136.20, 128.98, 126.68, 124.81, 119.95, 119.11, 116.39, 115.38, 115.27, 67.07, 63.10, 53.40, 37.79, 35.76, 31.90, 31.57, 31.04, 30.77, 29.78, 29.36, 29.06, 26.83, 23.14, 22.79, 14.29, 14.15. MALDI-TOF MS (*m*/*z*): $[M+H]^+$ calcd. for $C_{122}H_{128}Cl_4N_6O_2S_4$, 1979.7736; found, 1979.7763.

*Synthesis of **IPIC- 4F***

By employing the similar procedure as used for IPIC-4Cl, compound **5** (150.0 mg, 100.65 μmol) and 2F-IC (185.33 mg, 0.81 mmol) were used for the synthesis of IPIC-4F. The *title* compound was obtained as a green solid (154 mg, 80%). ^{1}H NMR (500 MHz, $CDCl_3$, δ): 8.82 (s, 2H), 8.49 (m, 2H), 7.62 (t, *J* = 7.5 Hz, 4H), 7.41 (s, 2H), 7.33-7.26 (m, 8H), 7.11 (d, *J* = 8.0 Hz, 8H), 3.63 (d, *J* = 8.2 Hz, 4H), 2.62-2.53 (m, 8H), 1.61-1.56 (m, 8H), 1.40-0.91 (m, 42H), 0.90-0.71 (m, 24H), 0.67-0.55 (m, 8H). ^{13}C NMR (125 MHz, $CDCl_3$, δ): 186.04, 158.96, 158.46, 155.29, 153.22, 152.17, 149.17, 146.75, 142.87, 139.59, 138.45, 137.50, 136.71, 136.13, 135.67, 134.59, 128.98, 126.93, 119.75, 119.27, 116.35, 115.26, 114.72, 112.47, 112.30, 67.05, 63.10, 53.36, 37.83, 35.76, 31.91, 31.57, 31.03, 30.77, 29.78, 29.37, 29.10, 26.86, 23.14, 22.80, 14.29, 14.15. ^{19}F NMR (470 MHz, $CDCl_3$) δ: -124.30 (d, *J* = 19.1 Hz), -125.42 (d, *J* = 19.3 Hz). MALDI-TOF MS (*m*/*z*): $[M+H]^+$ calcd. for $C_{122}H_{128}F_4N_6O_2S_4$, 1912.8918; found, 1912.8916.

*Synthesis of **IPIC***

By employing the similar procedure as used for IPIC-4Cl, compound **5** (150.0 mg, 100.65 μmol) and IC (156.36 mg, 0.81 mmol) were used for the synthesis of IPIC. The *title* compound was obtained as a black-green solid (128 mg, 69%). ^{1}H NMR (500 MHz, $CDCl_3$, δ): 8.85 (s, 2H), 8.66-8.61 (m, 2H), 7.86 (m, 2H), 7.73-7.51 (m, 7H), 7.40 (d, *J* = 2.8 Hz, 2H), 7.32-7.27 (m, 8H), 7.11 (d, *J* = 6.7 Hz, 9H), 3.63 (d, *J* = 8.2 Hz, 4H), 2.58 (t, *J* = 7.6 Hz, 8H), 1.59-1.56 (m, 8H), 1.38-0.90 (m, 42H), 0.90-0.73 (m, 24H), 0.67-0.56 (m, 8H). ^{13}C NMR (125 MHz, $CDCl_3$, δ): 188.47, 161.07, 158.24, 151.08, 148.41, 146.37, 142.76, 140.21, 139.55, 138.54,

137.65, 137.03, 136.57, 136.17, 134.68, 133.99, 129.01, 128.91, 126.55, 125.06, 123.47, 120.27, 119.49, 116.15, 115.68, 66.71, 63.05, 53.32, 37.81, 35.74, 31.90, 31.55, 31.02, 30.76, 29.77, 29.35, 29.08, 26.84, 23.14, 22.78, 14.28, 14.14. MALDI-TOF MS (m/z): $[M+H]^+$ calcd. for $C_{122}H_{132}N_6O_2S_4$, 1840.9295; found, 1840.9297.

2. Material Characterization

^1H and ^{13}C NMR spectra were recorded on a Bruker AVANCE III 500 MHz instrument with sample solutions in $CDCl_3$ using tetramethylsilane (TMS) as internal standard. The matrix-assisted laser desorption/ionization time-of-flight (MALDI-TOF) mass spectra were recorded on a Bruker Autoflex TOF/TOF spectrometer. Ultraviolet-visible (UV-Vis) absorption spectra were collected on a UV-Vis instrument Evolution 220 (Thermo Fisher). The thermogravimetric analyses (TGA) was performed on a TA instrument (Netzsch TG 209F1) with heating rate of 20 $^oC \cdot min^{-1}$ under nitrogen gas flow, with the temperature corresponding to 5% weight loss defined as the decomposition temperature (T_d). Cyclic voltammetry measurements were carried out on a CHI Instruments Model CHI 600D electrochemical workstation. All initial potentials were determined in tetrabutylammonium hexafluorophosphate (0.1 M anhydrous acetonitrile solution) under N_2 atmosphere at a scan rate of 50 $mV \cdot s^{-1}$ and corrected against Fc/Fc^+.

3. NMR and Mass Spectra

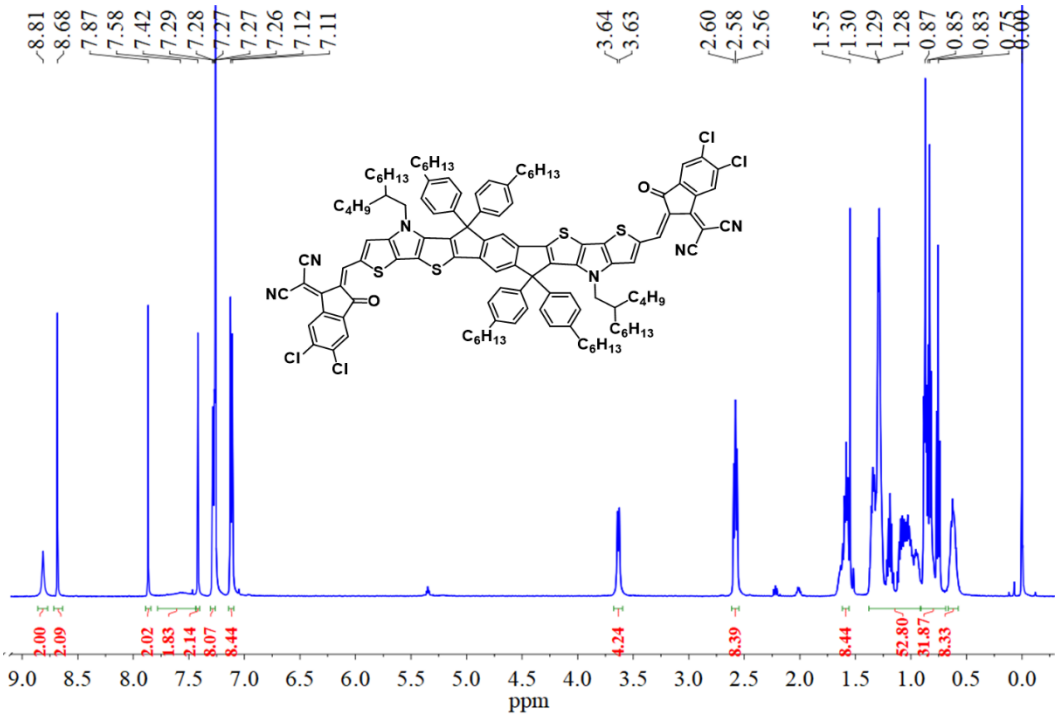

Figure S1. ^1H NMR spectrum of IPIC-4Cl.

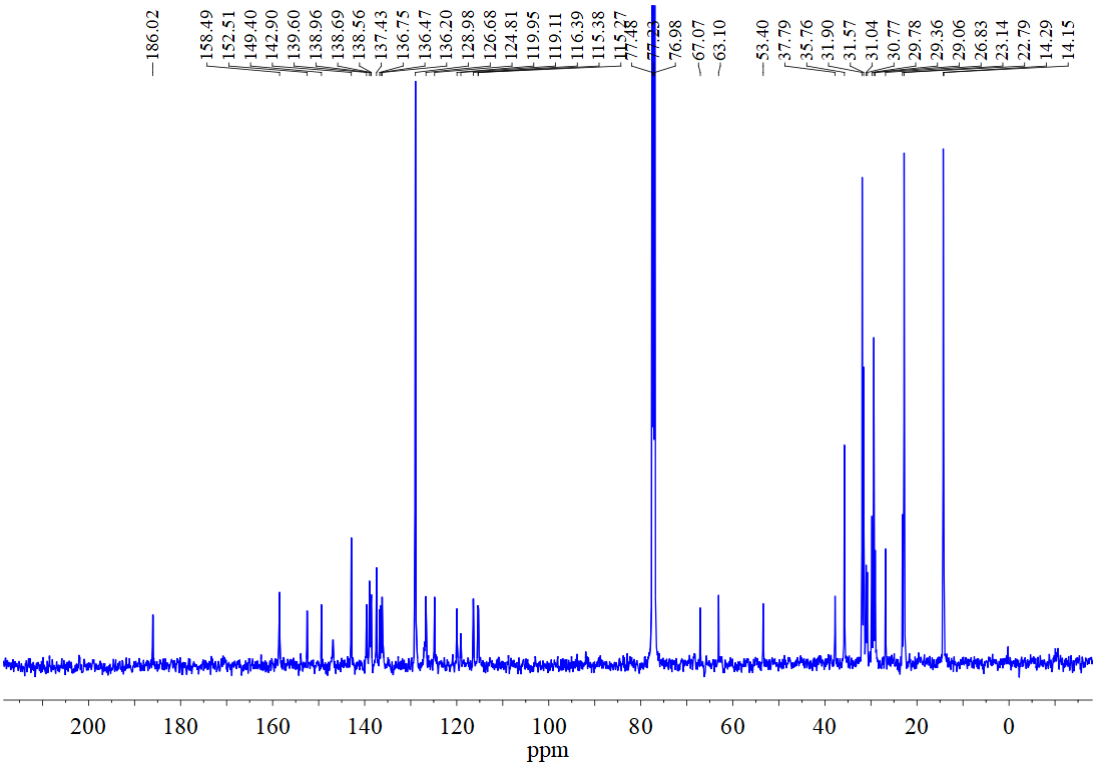

Figure S2. ^{13}C NMR spectrum of IPIC-4Cl.

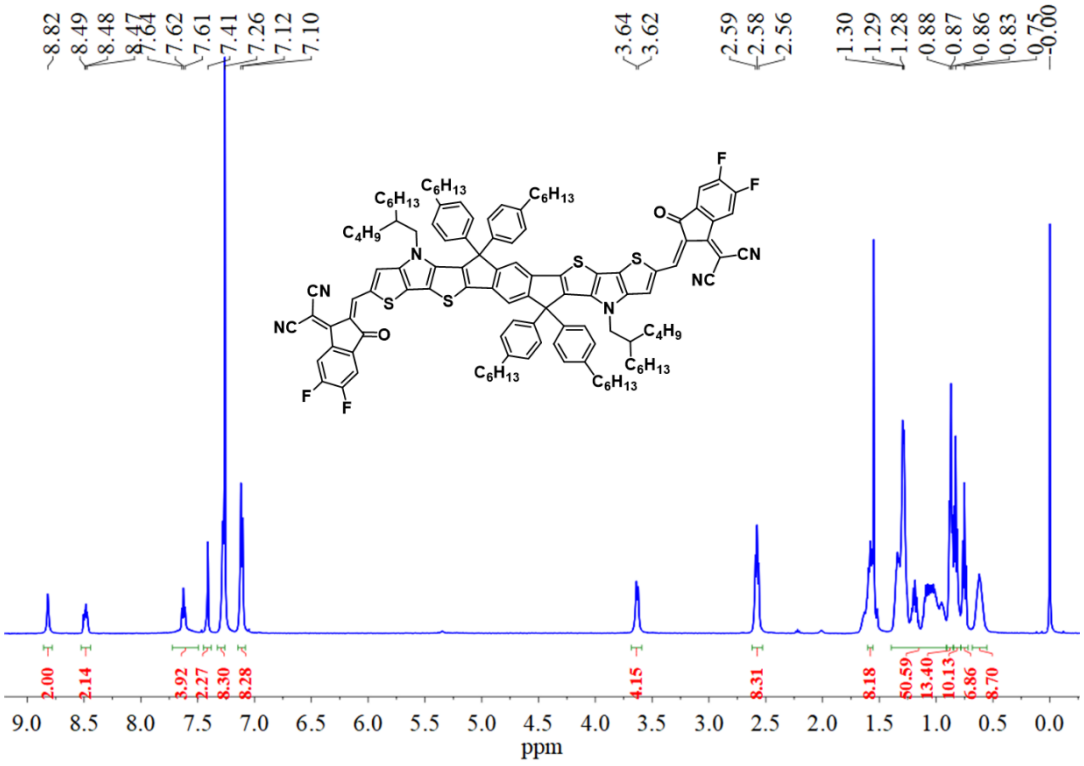

Figure S3. ^{1}H NMR spectrum of IPIC-4F.

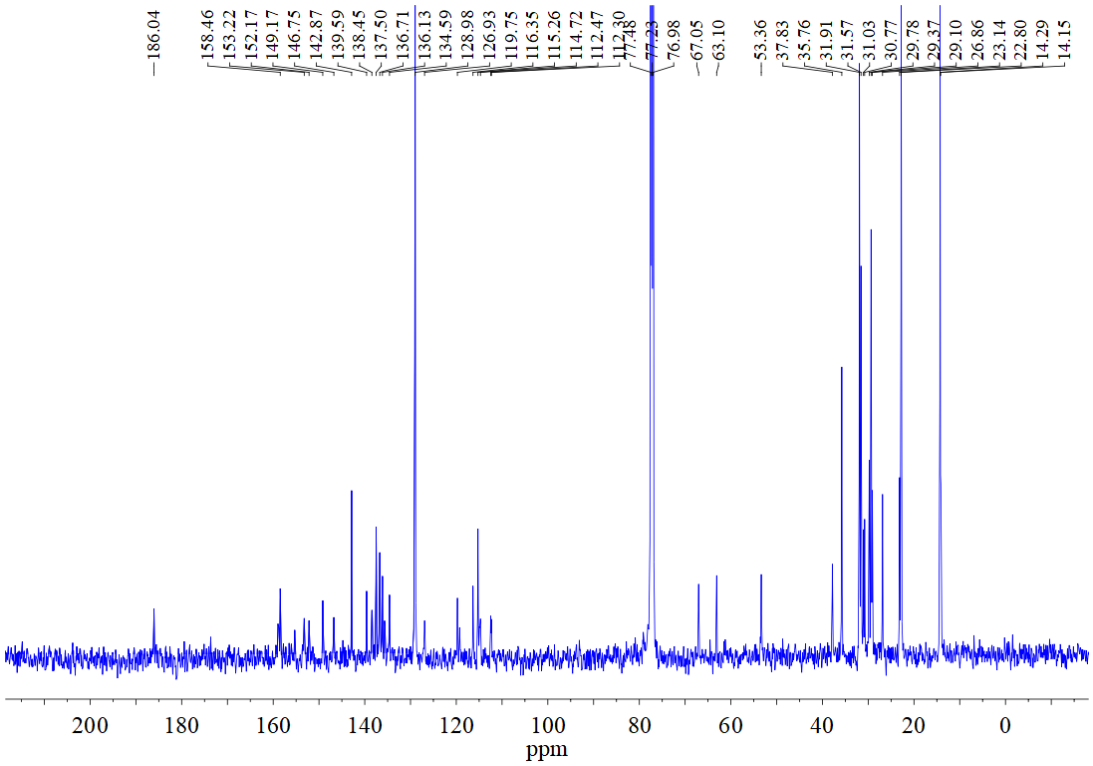

Figure S4. ^{13}C NMR spectrum of IPIC-4F.

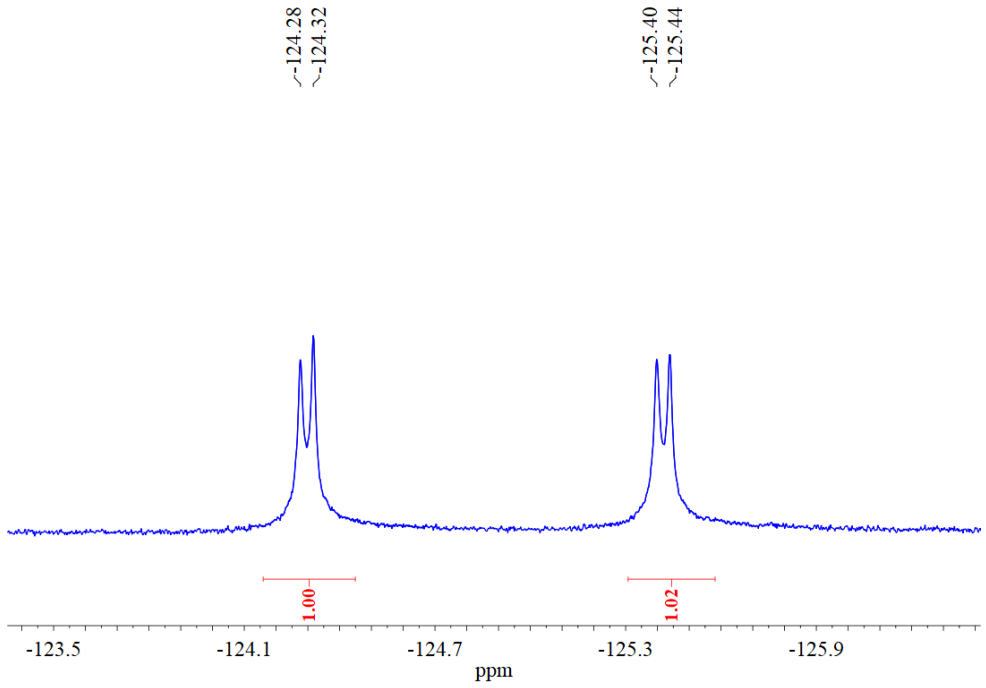

Figure S5. ^{19}F NMR spectrum of IPIC-4F.

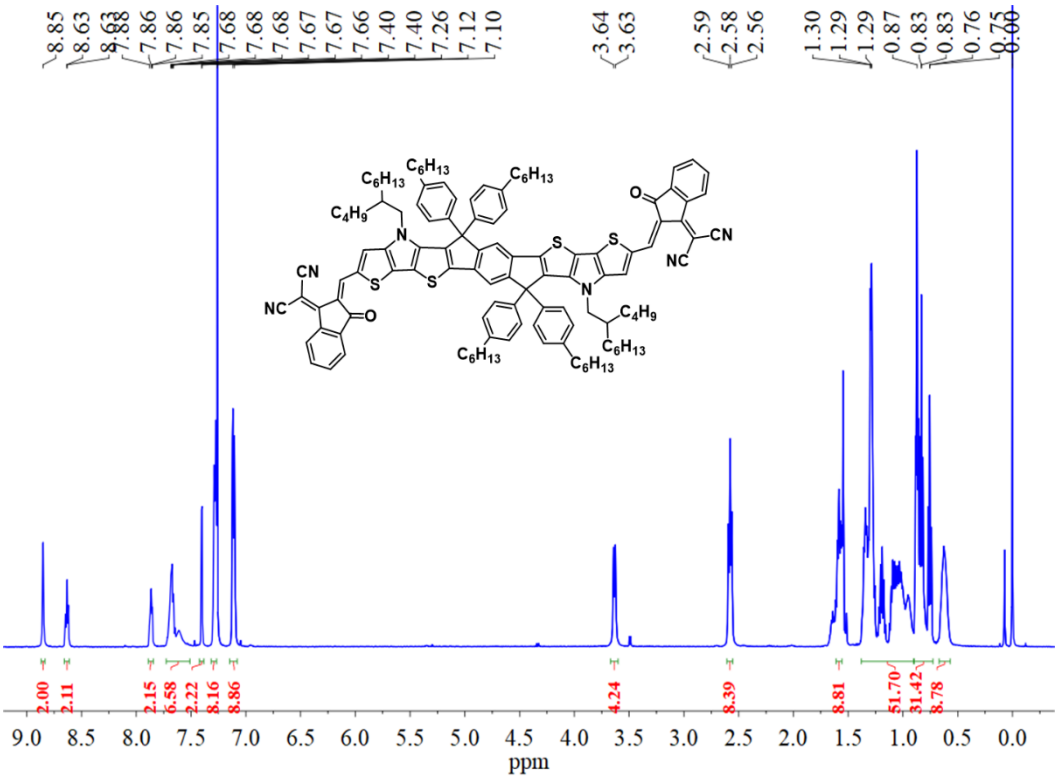

Figure S6. ^{1}H NMR spectrum of IPIC.

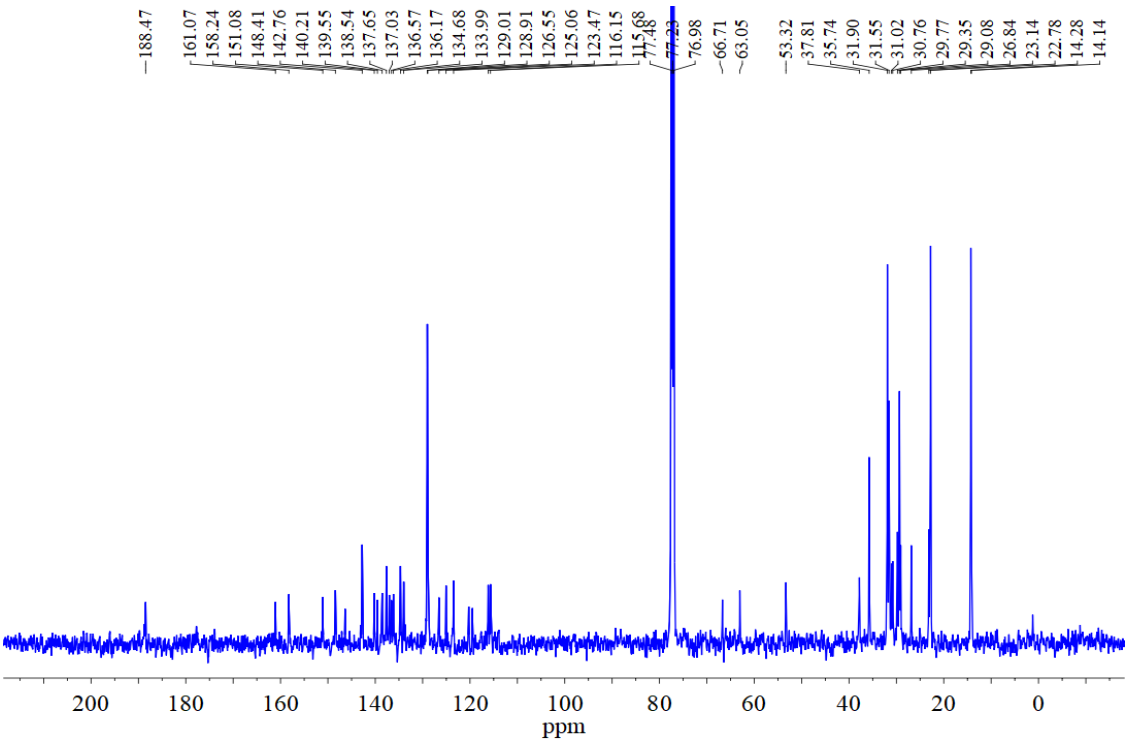

Figure S7. ^{13}C NMR spectrum of IPIC.

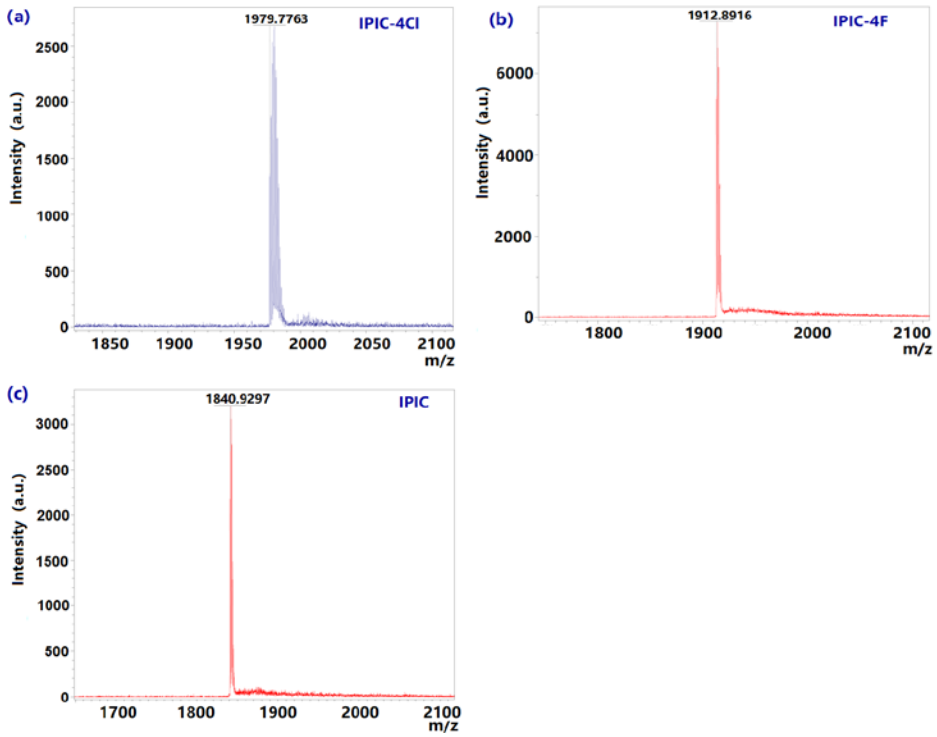

Figure S8. The MALDI-TOF MS plots of IPIC, IPIC-4F and IPIC-4Cl.

4. TG Analysis, UV-vis Absorption and CV measurement

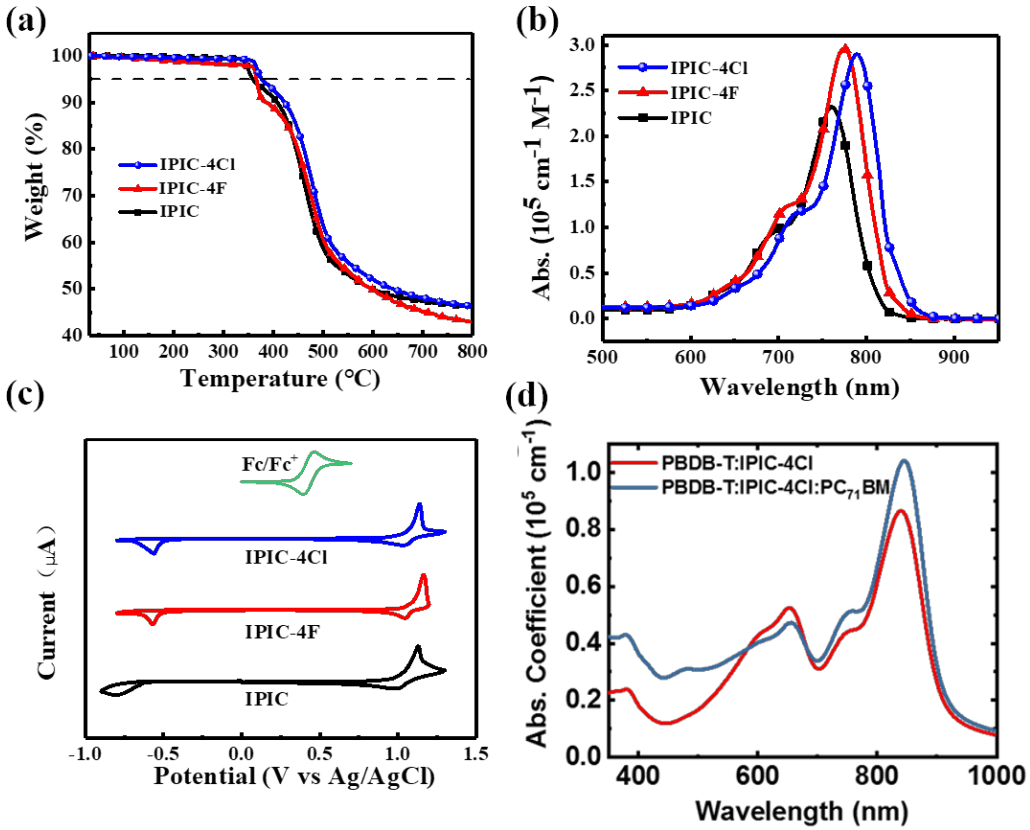

Figure S9. a) TGA traces and b) chloroform solution (10^{-5} M) absorption spectra of three acceptors; (c) CV traces of three acceptors; (d) Absorption profiles of binary and ternary blend films

5. Theoretical Modeling

Density functional theory (DFT) calculations with B3LYP/6-31G (d, p) basis set were performed to evaluate molecular conformations, energy levels and dipole moments, utilizing Gaussian 09. Particularly, *n*-hexyl and *n*-octyl groups were simplified as methyl to shorten the calculation time.

6. Device Fabrication and Measurements

The device structure is indium tin oxide (ITO)/poly(3,4-ethylenedioxythiophene)-poly(styrenesulfonate) (PEDOT:PSS)/active layer/(2-(1,10-phenanthrolin-3-yl)naphth-6-yl)diphenylphosphine oxid (Phen-NaDPO)/Ag. PBDB-T and Phen-NaDPO were purchased from 1-Materials, PEDOT:PSS was purchased from Heraeus. Phen-NaDPO was used as electron transport layer according to previous work.[S2] The non-fullerene acceptor (IPIC, IPIC-4F and IPIC-4Cl) and PBDB-T (weight ratio of 1:1) were dissolved in chlorobenzene with 0.5 % diiodooctane (DIO) addition, then the mixture was stirred at 80 ºC to obtain a blend solution with a total concentration of 20 mg/mL. The patterned ITO-coated glass substrates (15 Ω per square) were cleaned via sequential sonication in detergent, de-ionized and ethanol. The ITO substrates were then dried by using high pure nitrogen gas and treated by oxygen plasma for 5 minute to improve their work function and clearance. Subsequently, the PEDOT:PSS solution (Heraeus Clevios P VP A 4083) was spin-coated on ITO substrates at 4500 rounds per minute (RPM) for 30 s and annealed at 150 °C for 10 minutes in atmospheric air. The ITO substrates coated with PEDOT:PSS layer were transferred into a nitrogen-filled glovebox. The blend solution was spin-cast on the top of PEDOT: PSS layer at 2000 rmp for 30 s. Then it was annealed at 100 °C for 10 min. A thin Phen-NaDPO layer (8 nm) was spin-coated on top of the acitve layer. Then, the devices were transferred to evaporator chamber and Ag layer (100 nm) were sequentially evaporated under vacuum of 2×10^{-6} Torr through a shadow mask. The active area of each device was 0.1 cm^2 controlled by a shadow mask.

J-V measurements of solar cells were performed in the glovebox with a Keithley 2400 source meter and an Oriel Sol3A Class AAA solar simulator calibrated to 1 sun, AM1.5 G. The external quantum efficiency (EQE) measurements were performed at zero bias by illuminating the device with monochromatic light supplied from a Xenon arc lamp in combination with a dual-grating monochromator. The number of photons incident on the sample was calculated for each wavelength by using a silicon photodiode calibrated by NIST. Transmission electron microscopy (TEM) images of active layers were obtained by a FEI instrument at 300 kV accelerating voltage. A 5400 Agilent Atomic force microscopy (AFM) instrument was

performed to obtain morphology images.

In photo-CELIV measurements, the devices were illuminated with a 405 nm laser-diode. Current transients were recorded across an internal 50 Ω resistor of an oscilloscope (Agilent Technologies DSO-X 2024A). We used a fast electrical switch to isolate the cell and prevent charge extraction or sweep out during the laser pulse and the delay time. After a variable delay time, a linear extraction ramp is applied via a function generator. The ramp, which was 60 μs long and 2 V in amplitude, was set to start with an offset matching the V_{oc} of the cell for each delay time. The effective charge carrier mobility of organic thin film can be calculated by the equation below:

$$\mu = \frac{2d^2}{3At^2_{\max}\left[1+0.36\frac{\Delta j}{j_0}\right]} \quad if\ \Delta j \le j_0$$

where d is the active layer thickness, A is the voltage rise speed, $A = dU/dt$, U is the applied voltage, t_{max} is the time corresponding to the maximum of the extraction peak, j_0 is the displacement current and Δj is the transient current peak height.

In transient photocurrent (TPC) measurements, a 405 nm laser diode driven by the function generator was used to generate 100 ms light pulses. The current response was amplified with a transimpedance amplifier and recorded with a digital oscilloscope.

Table S1. Photovoltaic parameters of IPIC-4Cl based binary devices with different D/A weight ratio

D/A	J_{SC} [mA/cm^2]	V_{OC} [mV]	FF [%]	PCE [%]
1:0.5	19.4	829	59.4	9.57
1:1	20.5	824	59.9	10.1
1:1.5	20.2	800	57.2	9.11

Table S2. Photovoltaic parameters of IPIC-4Cl based binary devices with different additive content

volume ratio	J_{SC} [mA/cm^2]	V_{OC} [mV]	FF [%]	PCE [%]
0% DIO	20.5	824	59.9	10.1
0.5% DIO	21.6	825	65.2	11.6
1% DIO	19.4	820	71.0	11.3
2% DIO	17.5	827	63.3	9.15

Table S3. Photovoltaic parameters of IPIC-4Cl based binary devices with different thermal annealing temperature

Annealing [°C]	J_{SC} [mA/cm^2]	V_{OC} [mV]	FF [%]	PCE [%]
80	21.5	825	69.8	12.4
100	22.2	813	74.0	13.4
120	21.3	829	70.0	12.4
140	18.0	823	63.5	9.41

Table S4. Photovoltaic parameters of IPIC-4Cl based binary devices with different device structure

	J_{SC} [mA/cm^2]	V_{OC} [mV]	FF [%]	PCE[%]
Normal Structure	22.2	813	74.0	13.4
Inverted Structure	21.2	824	71.1	12.4

Table S5. Photovoltaic parameters of IPIC-4F based binary devices with different D/A weight ratio

D/A	J_{SC} [mA/cm^2]	V_{OC} [mV]	FF [%]	PCE [%]
1:0.5	18.5	840	68.0	10.6
1:1	19.8	835	67.1	11.1
1:1.5	17.1	844	67.8	9.79

Table S6. Photovoltaic parameters of IPIC based binary devices with different D/A weight ratio

D/A	J_{SC} [mA/cm^2]	V_{OC} [mV]	FF [%]	PCE [%]
1:0.5	5.62	944	57.3	3.04
1:1	7.16	950	58.6	3.98
1:1.5	6.72	961	57.2	3.69

Table S7. Photovoltaic parameters of IPIC-4Cl based ternary devices with different D/A weight ratio

PBDB-T:IPIC-4Cl:$PC_{71}BM$ (by weight ratio)	J_{SC} [mA cm^{-2}]	V_{OC} [mV]	FF [%]	PCE [%]
1:1:0	22.2	813	74.0	13.4
1:1:0.1	22.6	823	73.2	13.6
1:1:0.3	23.3	822	74.6	14.3
1:1:0.5	20.4	822	72.3	12.1

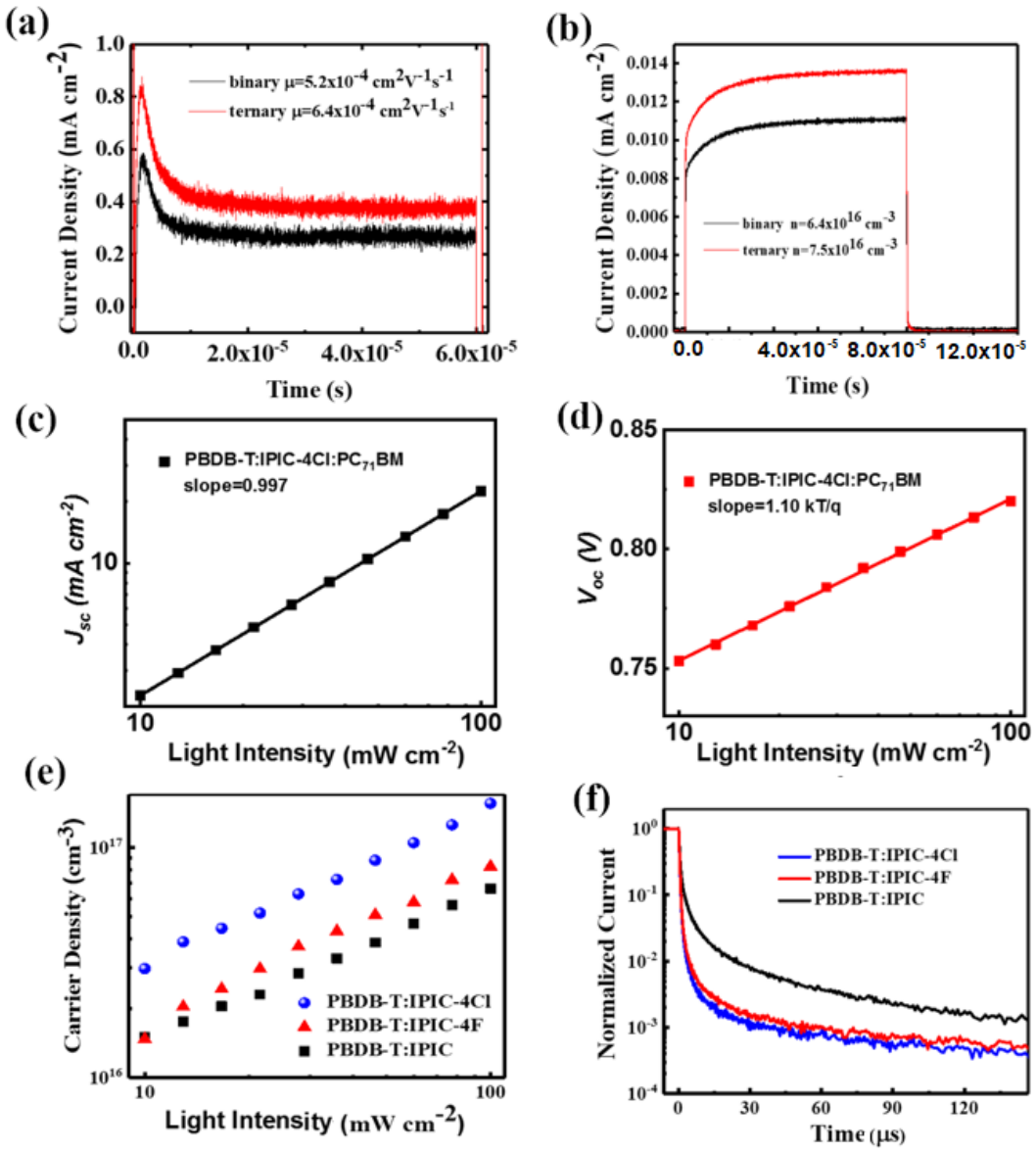

Figure S10. (a) The curves of Photo-CELIV in IPIC-4Cl based binary and ternary devices; (b) TPC measurements in IPIC-4Cl based binary and ternary devices; (c) J_{sc} versus light intensity of ternary devices; (d) V_{oc} versus light intensity of ternary devices; (e) Carrier density versus light intensity of designed devices; (f) The transient photocurrent curves of three OSCs.

7. SCLC Mobility Measurements

Electron-only devices with the structure of ITO/ZnO/Active layer/Ca/Al and hole-only devices with the structure of ITO/PEDOT:PSS/Active layer/MoO_x/Ag were used to evaluate charge mobility by SCLC model. The charge mobility can be determined based on the Mott-Gurney equation with Poole-Frenkel correction:

$$J = \frac{9}{8}\varepsilon_r\varepsilon_0\mu\frac{V^2}{d}\exp\left[0.89\gamma\sqrt{\frac{V}{d}}\right] \quad (1)$$

here, ε_r is dielectric constant of organic materials, ε_0 is the free space permittivity, d is the

thickness of active layer, μ is the charge carrier mobility, and V is the applied voltage.

Table S8. Hole and electron mobilities of the blend films.

Blend film	μ_h[cm^2 V^{-1} s^{-1}]	μ_e[cm^2 V^{-1} s^{-1}]	μ_h/μ_e
PBDB-T/IPIC-4Cl/PC$_{71}$BM (1:1:0.3)	2.73×10^{-4}	2.68×10^{-4}	1.02
PBDB-T/IPIC-4Cl	1.26×10^{-4}	1.00×10^{-4}	1.26
PBDB-T/IPIC-4F	1.22×10^{-4}	5.61×10^{-5}	2.17
PBDB-T/IPIC	5.72×10^{-5}	2.53×10^{-7}	226

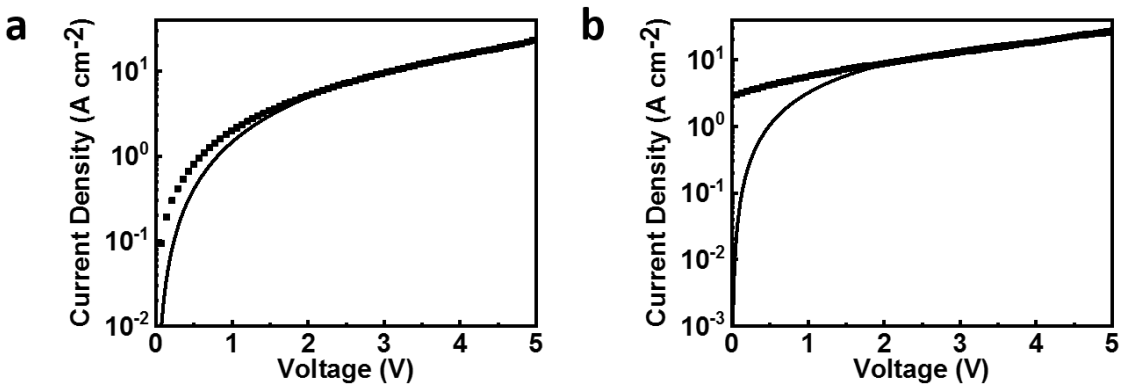

Figure S11. The hole (a) and electron (b) mobility of the ternary blend film.

8. Morphology Characterization

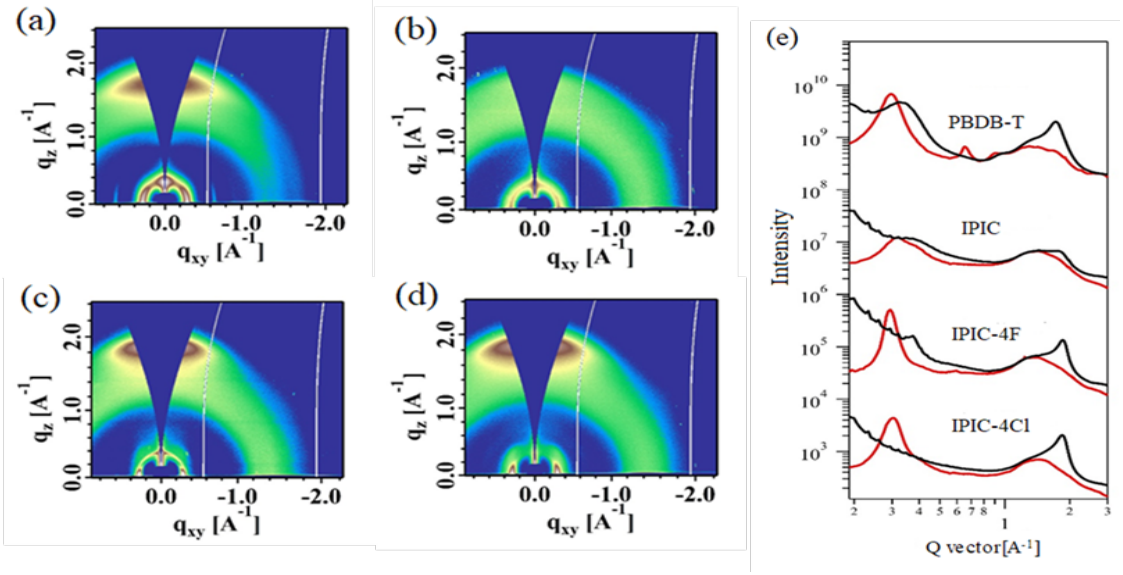

Figure S12. GIWAXS of pure films: a) PBDB-T, b) IPIC, c) IPIC-4F, d) IPIC-4Cl. e) In-plane (red line) and out-of-plane (black line) line-cut profiles of GIWAXS patterns.

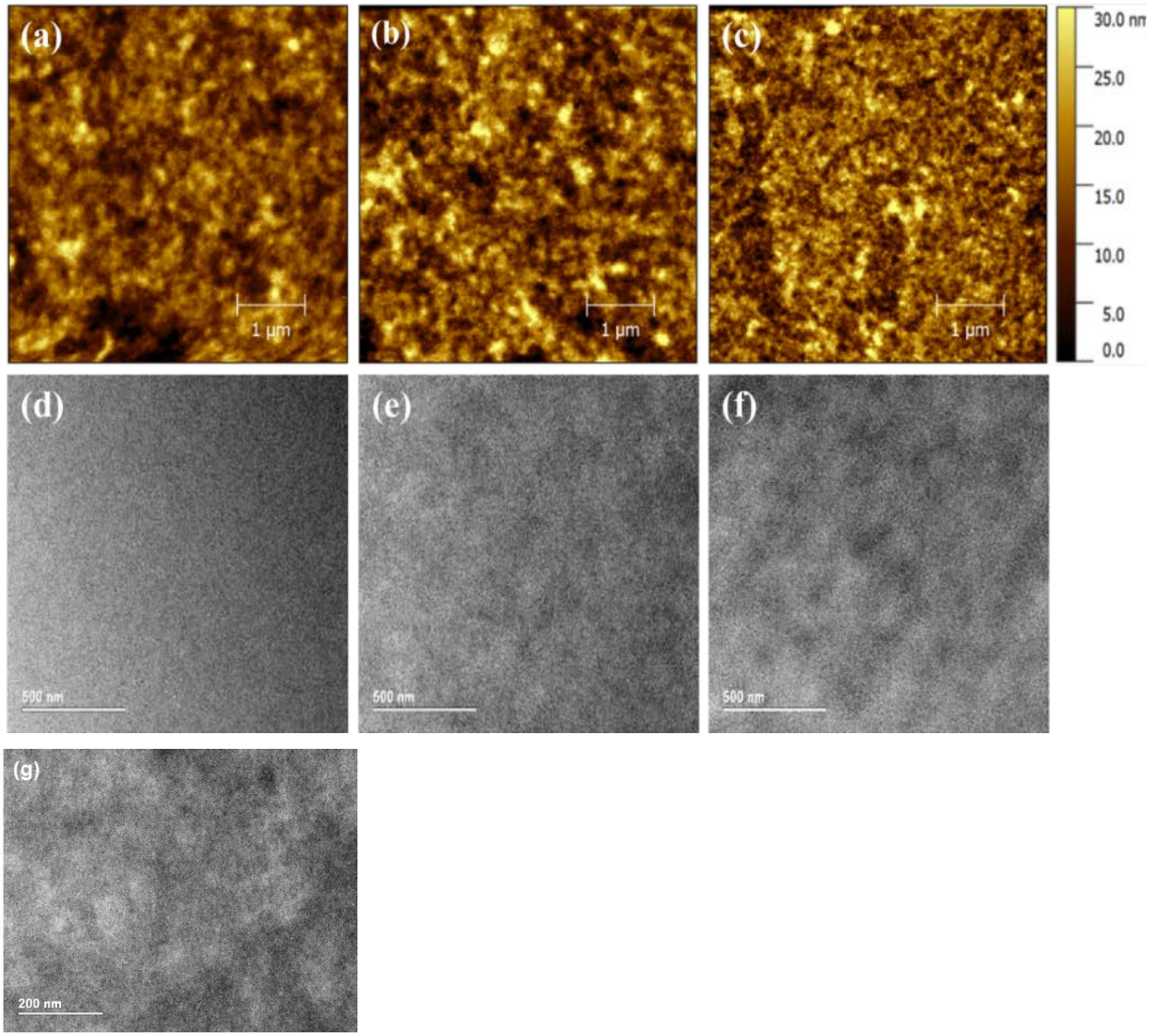

Figure S13. AFM and TEM images of PBDB-T:IPIC-4Cl (a,d), PBDB-T:IPIC-4F (b,e) and PBDB-T:IPIC blend films (c,f), (g) TEM image of PBDB-T:IPIC-4Cl:$PC_{71}BM$ ternary blend.

9. Summary of photovoltaic data for representative NFAs based devices in Literature

Table S9 Photovoltaic data for representative chlorinated NFAs based binary devices

Active layer	J_{sc} [mA/cm^2]	V_{oc} [mV]	FF [%]	PCE [%]	E_g^{opt} [eV]	E_{loss} [eV]	Reference
PBDB-T:**IEICO-4Cl**	20.8	744	62.5	9.67	1.23	**0.49**	[S1]
PTB7-Th:**IEICO-4Cl**	22.8	727	62.0	10.3	1.23	**0.50**	[S1]
PBDB-T**:IPIC-4Cl**	22.2	813	74.0	13.4	1.32	**0.51**	This work
J52:**IEICO-4Cl**	23.8	700	60.7	10.1	1.23	**0.53**	[S1]
PBDB-T-SF:**NCBDT-4Cl**	22.4	851	74.3	14.1	1.40	**0.55**	[S3]
PBDB-T:**IXIC-4Cl**	22.9	690	71.2	11.2	1.25	**0.56**	[S4]
PBDB-T:**IXIC-2Cl**	23.6	730	70.9	12.2	1.30	**0.57**	[S4]
DRTB-T:**F-2Cl**	17.2	969	64.4	10.8	1.54	**0.57**	[S5]
PCE-10:**BT-CIC**	22.5	700	71.0	11.2	1.30	**0.60**	[S6]
PTPDBDT:**Cl-ITIC**	15.6	940	65.0	9.50	1.56	**0.62**	[S7]
DRCN5T:**F-2Cl**	16.0	906	68.4	9.89	1.54	**0.63**	[S5]
PBDB-T-2F:**IT-2Cl**	19.1	922	74.8	13.2	1.55	**0.63**	[S8]
PBDB-T-2F:**IT-4Cl**	22.7	790	75.2	13.5	1.48	**0.69**	[S8]
PBDB-T:**F-Cl**	17.6	870	75.0	11.5	1.58	**0.71**	[S9]

Table S10 Summary of representative NFAs with PCE over 14%

Active layer	J_{sc} [mA/cm^2]	V_{oc} [mV]	FF [%]	PCE [%]	Reference	Device structure
PM6:**Y6**	25.2	820	76.1	**15.7**	[S10]	**Binary**
PBDB-TF:**IT-4F**	20.7	870	80.8	**14.6**	[S11]	
PBDB-T-2Cl:**IT-4F**	21.8	860	77.0	**14.4**	[S12]	
PBDB-T-2Cl:**IT-4F**	20.6	890	78.0	**14.3**	[S13]	
PDTB-EF-T:**IT-4F**	20.7	900	76.0	**14.2**	[S14]	
PBDB-T-SF:**NCBDT-4Cl**	22.4	851	74.3	**14.1**	[S3]	
PTB7-Th:**CO$_i$8DFIC**:PC$_{71}$BM	27.4	727	73.4	**14.6**	[S15]	**Ternary**
PBDB-T:IPIC-4Cl:PC$_{71}$BM	23.3	822	74.6	**14.3**	This work	
PBDB-T-2F:**IT-4Cl**:**IT-2Cl**	22.0	842	76.4	**14.2**	[S8]	
PM6:ITCPTC:**MeIC**	18.4	981	78.2	**14.1**	[S16]	
PTB7-Th:**CO$_i$8DFIC**:PC$_{71}$BM	28.2	700	71.0	**14.1**	[S17]	
PBDB-T: **F-M** / PTB7-Th: **NOBDT**	11.7	1.71	70.0	**14.1**	[S18]	**Tandem**
PBD1:PC$_{71}$BM/ PTB7-Th:**IEICO-4F**	12.3	1.61	72.0	**14.2**	[S19]	
DTDCPB:C$_{70}$/ PCE-10:**BT-CIC**	13.3	1.59	71.0	**15.0**	[S20]	
DTDCPB:C$_{70}$/ PCE-10:**BT-CIC**:**TT-FIC**	13.8	1.56	71.0	**15.4**	[S21]	
PBDB-T:**F-M**/ PTB7-Th:**CO$_i$8DFIC**:PC$_{71}$BM	14.4	1.64	73.7	**17.4**	[S22]	

Reference

[S1] Cui Y.; Yang C.; Yao H.; Zhu J.; Wang Y.; Jia G.; Gao F.; Hou J. Efficient Semitransparent Organic Solar Cells with Tunable Color enabled by an Ultralow-Bandgap Nonfullerene Acceptor. *Adv. Mater.* **2017**, 29, 1703080.

[S2] Liang R.; Babics M.; Savikhin V.; Zhang W.; Corre V.; Lopatin S.; Kan Z.; Firdaus Y.; Liu S.; McCulloch I.; Toney M.; Beaujuge P. Carrier Transport and Recombination in Efficient "All-Small-Molecule" Solar Cells with the Nonfullerene Acceptor IDTBR. *Adv. Energy Mater.* **2018**, 8, 1800264.

[S3] Kan B.; Feng H.; Yao H.; Chang M.; Wan X.; LiC.; Hou J.; Chen Y. A chlorinated low-bandgap small-molecule acceptor for organic solar cells with 14.1% efficiency and low energy loss. *Sci. China Chem*. **2018**, 61, 1307-1313.

[S4] Chen Y.; Liu T.; Hu H.; Ma T.; Lai J. Y. L.; Zhang J.; Ade H.; Yan H. *Adv. Energy Mater.* **2018**, 8, 1801203.

[S5] Wang Y.; Wang Y.; Kan B.; Ke X.; Wan X.; Li C.; Chen Y. High-Performance All-Small Molecule Solar Cells Based on a New Type of Small Molecule Acceptors with Chlorinated End Groups. *Adv. Energy Mater.* **2018**, 8, 1802021.

[S6] Li Y.; Lin J. D.; Che X.; Qu Y.; Liu F.; Liao L. S.; Forrest S. R. High Efficiency Near-Infrared and Semitransparent Non-Fullerene Acceptor Organic Photovoltaic Cells. *J. Am. Chem.Soc.* **2017**, 139, 17114-17119.

[S7] Yang F.; Li C.; Lai W.; Zhang A.; Huang H.; Li W. Halogenated Conjugated Molecules for Ambipolar Field-Effect Transistors and Non-Fullerene Organic Solar Cells. *Mater. Chem. Front.* **2017**, 1, 1389.

[S8] Zhang H.; Yao H.; Hou J.; Zhu J.; Zhang J.; Li W.; Yu R.; Gao B.; Zhang S.; Hou J. Over 14% Efficiency in Organic Solar Cells Enabled by Chlorinated Nonfullerene Small-Molecule Acceptors. *Adv. Mater.* **2018**, 30, 1800613.

[S9] Wang Y.; Zhang Y.; Qiu N.; Feng H.; Gao H.; Kan B.; Y Ma.; Li C.; Wan X.; Chen Y. A Halogenation Strategy for over 12% Efficiency Nonfullerene Organic Solar Cells. *Adv. Energy Mater.* **2018**, 8, 1702870.

[S10] Yuan J.; Zhang Y.; Zhou L.; Zhang G.; Yip H.; Lau T.; Lu X.; Zhu C.; Peng H.; Johnson P.; Leclerc M.; Cao Y.; Ulanski J., Li Y.; Zou Y. Single-Junction Organic Solar Cell with over 15% Efficiency Using Fused-Ring Acceptor with Electron-Deficient Core. *Joule* **2019**, DOI: 10.1016/j.joule.2019.01.004.

[S11] Zheng Z.; Hu Q.; Zhang S.; Zhang D.; Wang J.; Xie S.; Wang R.; Qin Y.; Li W.; Hong L.; Liang N.; Liu F.; Zhang Y.; Wei Z.; Tang Z.; Russell T.; Hou J., Zhou H. A Highly

Efficient Non-Fullerene Organic Solar Cell with a Fill Factor over 0.80 Enabled by a Fine-Tuned Hole-Transporting Layer. *Adv. Mater.* **2018**, 30, 1801801.

[S12] Zhang S.; Qin Y.; Zhu J.; Hou J. Over 14% Efficiency in Polymer Solar Cells Enabled by a Chlorinated Polymer Donor. *Adv. Mater.* **2018**, 30, 1800868.

[S13] Zhang Y.; Yao H.; Zhang S.; Qin Y.; Zhang J.; Yang L.; Li W.; Wei Z.; Gao F.; Hou J. Fluorination vs. Chlorination: a Case Study on High Performance Organic Photovoltaic Materials. *Sci. China Chem.* **2018**, 61, 1328-1337.

[S14] Li S.; Ye L.; Zhao W.; Yan H.; Yang B.; Liu D.; Li W.; Ade H.; Hou J. A Wide Band Gap Polymer with a Deep Highest Occupied Molecular Orbital Level Enables 14.2% Efficiency in Polymer Solar Cells. *J. Am. Chem. Soc.* **2018**, 140, 7159-7167.

[S15] Li H.; Xiao Z.; Ding L.; Wang J. Thermostable Single-Junction Organic Solar Cells with a Power Conversion Efficiency of 14.62%. *Sci. Bull.* **2018**, 63, 340-342.

[S16] Liu T.; Luo Z.; Fan Q.; Zhang G.; Zhang L.; Gao W.; Guo X.; Ma W.; Zhang M.; Yang C.; Li Y.; Yan H. Use of Two Structurally Similar Small Molecular Acceptors Enabling Ternary Organic Solar Cells with High Efficiencies and Fill Factors. *Energy Environ. Sci.*, **2018**, 11, 3275-3282

[S17] Xiao Z.; Jia X.; Ding L. Ternary Organic Solar Cells Offer 14% Power Conversion Efficiency. *Sci. Bull.* **2017**, 62, 1562-1564.

[S18] Zhang Y.; Kan B.; Sun Y.; Wang Y.; Xia R.; Ke X.; Yi Y.; Li C.; Yip H.; Wan X.; Cao Y.; Chen Y. Nonfullerene Tandem Organic Solar Cells with High Performance of 14.11%. *Adv. Mater.* **2018**, 30, 1707508.

[S19] Guo B.; Li W.; LuoG .; Guo X.; Yao H.; Zhang M.; Hou J.; Li Y.; Wong W. Exceeding 14% Efficiency for Solution-Processed Tandem Organic Solar Cells Combining Fullerene- and Nonfullerene-Based Subcells with Complementary Absorption. *ACS Energy Lett.*, **2018**, 3, 2566-2572.

[S20] Che X.; Li Y.; Qu Y.; Forrest S. High fabrication yield organic tandem photovoltaics combining vacuum- and solution-processed subcells with 15% efficiency. *Nat. Energy* **2018**, 3, 422-427.

[S21] Li Y.; Lin J.; Liu X.; Qu Y.; Wu F.; Liu F.; Jiang Z.; Forrest S. Near-Infrared Ternary Tandem Solar Cells. *Adv. Mater.* **2018**, 30,1804416.

[S22] Meng L.; Zhang Y.; Wan X.; Li C.; Zhang X.; Wang Y.; Ke X.; Xiao Z.; Ding L.; Xia R.; Yip H.; Cao Y.; Chen Y. Organic and Solution-Processed Tandem Solar Cells with 17.3% Efficiency. *Science* **2018**, 361, 1094-1098.